University of Oklahoma

Graduate College

DEVELOPMENT AND CHARACTERIZATION OF ADVANCED NANOCOMPOSITES WITH ENHANCED MECHANICAL AND THERMAL PROPERTIES

A THESIS

SUBMITTED TO THE GRADUATE FACULTY

in partial fulfillment of the requirements for

Degree of

MASTER OF SCIENCE

By

LANE TAYLOR

Norman, Oklahoma

2023

DEVELOPMENT AND CHARATERIZATION OF ADVANCED NANOCOMPOSITES WITH ENHANCED MECHANICAL AND THERMAL PROPERTIES

A THESIS APPROVED FOR THE SCHOOL OF AREOSPACE AND MECHANICAL ENGINEERING

BY THE COMMITTEE CONSISTING OF

Dr. Yingtao Liu

Dr. Kuang-Hua Chang

Dr. Jivtesh Garg

Table of Contents

Table of Figures

Table of Tables

Abstract

The mechanical and thermal properties of composites made of polydimethylsiloxane (PDMS), glass micro-balloons (GmBs), and carbon nanotubes (CNTs) were investigated in this thesis. The objective of this study was to determine the effects of varying concentrations of GmBs and CNTs on the mechanical, resistive, and thermal behavior of the composites. The experimental approach involved preparing composite samples using a casting method, where the PDMS polymer was mixed with a fixed 1.25% of CNTs and varying concentrations of GmBs. The mixing and casting process was carefully crafted to ensure no GmBs were crushed during the process and to allow for quality samples to be produced for more accuracy during testing. Next, the samples were then subjected to mechanical and thermal tests to evaluate their properties. The mechanical properties were evaluated using two main types of tensile tests, testing until fracture and cyclic testing. During these tests the resistivity properties were measured to determine the max resistance change and the repeatability of the resistance measurements. The thermal properties were evaluated using LFA technology to determine the thermal diffusivity and to calculate thermal conductivity. Finally, the resistance was measured while the sample underwent heating to determine the effects of temperature on resistance. The results of the study showed that the incorporation of GmBs and CNTs in PDMS improved and can alter the mechanical, resistive, and thermal properties of the composite material. The addition of GmBs resulted in a significant decrease of the thermal conductivity while increasing the resistance change during tensile tests. Those samples with the highest loadings of GmBs had the best resistance stability at the widest temperature range. The combination of GmBs and CNTs resulted in a synergistic

effect, where the material properties of the composite were enhanced to a greater extent than when either component was added alone. Overall, these experiments added valuable insight to the abilities of CNT and GmB composites, but farther testing can still be completed. Testing higher loadings of GmBs would be very beneficial but more complex mixing methods would be required. Since the CNT loadings remained constant, varying the CNT amount could possibly make the material properties more favorable for different applications.

CHAPTER 1: INTRODUCTION

1.1: Composites and the benefits of nano-composites:

The most common materials in the engineering field are simple homogenous materials. These materials consist of a single type of material and have constant properties throughout them, such as density, strength, and specific heat. Some examples of homogenous materials include plastics, metals, and ceramics seen in Figure 1. Unlike homogenous materials, composite materials are comprised of two or more materials combined to make a single composite. The raw materials combined or the technique they are combined can alter and improve material characteristics and properties. Some materials in the composite family, as seen in Figure 2, include carbon fiber reinforced polymers, steel reinforced concrete, and plywood. A key difference between homogeneous and composite materials is composites have varying properties throughout, while homogeneous materials have constant properties.

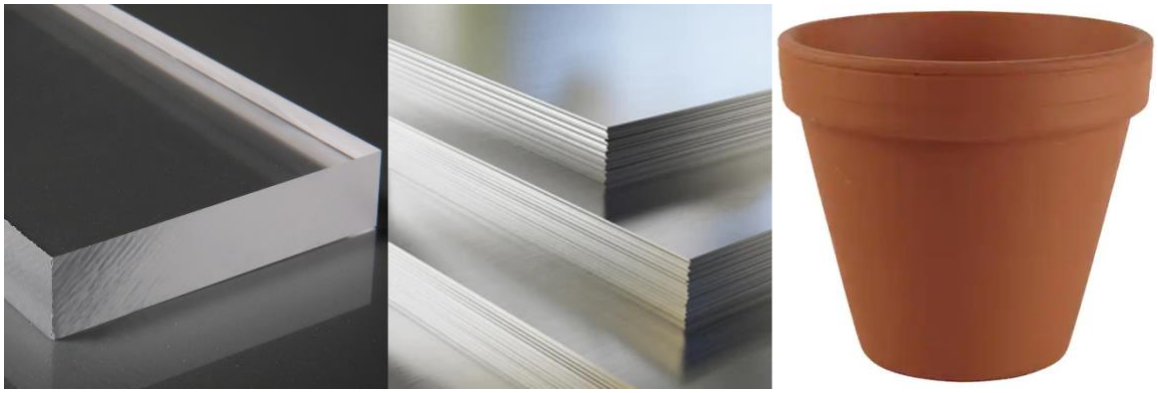

Figure 1: Homogeneous Materials (plastic, metal, ceramic)

Figure 2: Composite Materials (Carbon fiber, steel reinforced concrete, plywood)

Composites can be used in a variety of different applications and are commonly used when high strength is needed but weight savings are critical. The most common and adopting industry of composites is the aerospace industry. Composite materials allow for extremely high strength to weight ratio materials to be incorporated in aircraft structures [1, 2]. The weight savings allow for higher efficiency airplanes thus reducing fuel consumption to lower cost and environmental impact. Similar to aerospace, the automotive industry has also implemented composite materials. Automakers have used the increased strength to better protect the driver and passengers while simultaneously increasing the efficiency of the car [3, 4]. Due to the beneficial functionalities provided by composites and nanocomposites, the development aerospace structural materials can be extended to advanced applications, including damage detection, structural health monitoring, energy storage, autonomous deicing, and self-healing [5-12]. Using steel reinforced concrete mentioned earlier, the construction industry has revolutionized the ability to build complex structures. The addition of steel in concrete significantly increases the strength allowing for larger and safer infrastructure to be created. In the modern day, all roads and bridges utilize steel

reinforced concrete as well as concrete constructed buildings [13, 14]. The medical field also uses composite materials to provide better treatment and medical devices for patients [15-18]. Since the material properties can be altered, biocompatibility can be enhanced to produce better prosthetics and implants to increase the chances of success during the operation or treatment [19-22].

Nano and micro particles have been gaining increasing attention in the field of composite material research. These tiny particles have the potential to significantly improve the properties of composite materials. The reason for this is that using smaller particles leads to a higher surface area to volume ratio, which results in better mechanical and thermal properties of the composite [23-26]. This is because the transfer of loads and heat among smaller particles is more efficient compared to larger particles. The homogeneous distribution of additives is also achievable with smaller particles. The incorporation of electrically or thermally conductive particles can further enhance the properties of the composite material. The optimal utilization of the conductivity of these particles is made possible due to their even distribution within the composite matrix [27-30]. As a result, the use of small particles can lead to superior performance in a wide range of applications, including electronic packaging, heat sinks, as well as electrical and thermal insulation.

1.2: Overview of PDMS, CNT, and GmB

Polydimethylsiloxane, also called PDMS, is a silicone polymer that is known for excellent mechanical, thermal, chemical, and biocompatibility properties. PDMS is a highly flexible and rubber-like material that has high transparency and is odorless. PDMS also has exceptional resistance to heat, chemicals, and UV radiation, while also being a good electrical insulator. As a result of these outstanding characteristics, PDMS is known as a versatile material with a broad range of applications. Due to the high tensile strength of PDMS, the material is often used in soft robotics and microfluidic devices and other applications where flexibility and strength are key [31-33]. Furthermore, the excellent thermal properties allow PDMS to be used in high temperature environments and can act as thermal interface barriers. High chemical resistance makes PDMS an excellent choice when producing coating or sealants for other less resistant materials.

Carbon Nano Tubes, known as CNTs, are cylindrical structures made of highly organized carbon molecules typically 1-100 nanometers in diameter. CNTs can be produced in two different main forms, single and multi-walled, corresponding to the number of carbon layers in the cylinder. In recent years carbon nano tubes have been heavily researched due to their extreme material properties. CNTs have an extremely high tensile strength, roughly 100 times greater than steel, while also remaining very light [34]. The incredible strength to weight ratio allows CNTs to be used in a variety of applications. In addition to the high strength, CNTs are also very thermally

and electrically conductive making them very useful in electronics and high temperature environments [35]. The size of the CNTs creates a very high surface area ratio allowing them to be excellent at absorbing energy such as in batteries.

The final additive to be discussed is glass micro-balloons also known as GmB. GmB are micro sized hollow spheres ranging from 10 to 100μm in diameter. The thickness of the sphere walls is extremely thin allowing for the particles to have a very low density making them ideal to reduce existing composite densities [36]. Since GmBs are made of glass, the excellent thermal properties of glass are transferred to the GmBs which enable them to be used in thermal insulative applications [37].

1.3: What composites will be investigated

This study involves the investigation of various composite material compositions, aiming to evaluate the potential benefits and drawbacks of combining polydimethylsiloxane with carbon nanotubes and glass micro-balloons. In particular, the base material will be PDMS, and the CNT and GmB additives will be introduced at varying concentrations to form five unique compositions, each with a specific weight percentage of GmBs (0%, 5%, 10%, 15%, and 20%). CNTs will be introduced into the mixture at 1.25% weight and will remain constant across all compositions. This study holds significant importance in the field of materials science as it seeks

to reveal the effects of introducing CNT and GmB into PDMS, and to determine the respective strengths and weaknesses of the resultant composite materials. By conducting a thorough examination of each composition, this research will contribute to our understanding of how varying concentrations of these additives can influence the properties of PDMS and lead to the development of novel composite materials with improved characteristics.

CHAPTER 2: SAMPLE PRODUCTION

2.1: Introduction

The preparation of samples is a crucial process that involves a sequence of five steps. The first step is to accurately measure and mix the appropriate weight percentages of Carbon Nanotubes (CNTs) and Micro-Glass Balloons (GmB) into Polydimethylsiloxane (PDMS). This step requires precision to ensure that the resulting material has the desired properties and characteristics. Next, the mixed material is cast into molds, requiring careful handling to ensure even distribution of the mixture throughout the mold. After casting, the molds are then placed in an oven to undergo the curing process. The curing process involves a precisely controlled temperature and duration to ensure optimal cross-linking of the PDMS matrix. Once the curing process is complete, the material is carefully removed from the molds to prevent the sample from ripping or tearing. This step is critical in maintaining the integrity of the sample and ensuring accurate results. Finally, the cast material is cut into the desired sample shapes using a various stamping die, ensuring that each sample shape is consistent and uniform. Each step requires great attention to detail and

precision to ensure that the resulting samples have the desired properties and are suitable for accurate testing and analysis. The entire process can be summarized in Figure 3.

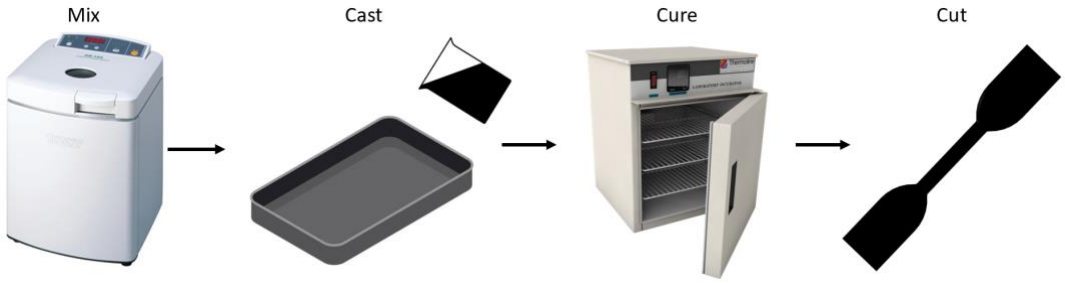

Figure 3: Sample Production Process

2.2: The Mixing Process

Starting with mixing, three main types of mixing are used in combination. First is using a metal spatula to hand mix the material. A centrifugal mixer is used to evenly disperse the nano and micro particles. A Kitchen Aide planetary mixer is used to mix in high loadings of micro glass balloons.

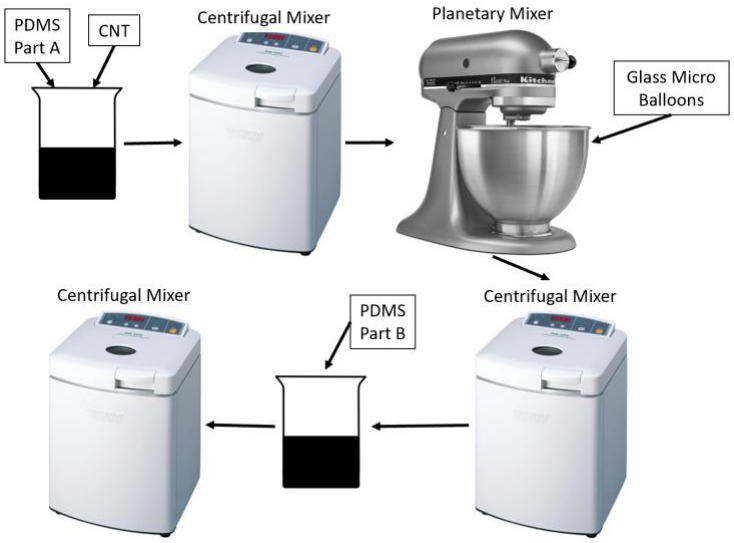

Figure 4: The Mixing Process

The mixing process outlined in Figure 4 begins by carefully measuring and dispensing the PDMS part A and CNTs into a plastic beaker. A metal spatula is then used to hand mix the two components thoroughly. The beaker is then placed into a centrifugal mixer for a duration of 10 minutes to ensure further dispersion of the CNTs. Next, the material is scooped into the stainless-steel bowl of the planetary mixer. The addition of micro glass balloons must be a slow to avoid them floating in the air or static electricity causing adhesion to the mixing bowl. Once all micro glass balloons have been added, the material is scooped back into the plastic beaker. The beaker is then returned to the centrifugal mixer for 3 minutes, ensuring not to overmix the micro glass balloons to avoid the risk of crushing and resulting in failed samples. After the addition of the PDMS part B, the mixture is once again hand mixed using a metal spatula to ensure

homogeneity. The beaker is then placed back into the centrifugal mixer for 3 more minutes to disperse part B evenly throughout the mixture.

2.3: Casting

Following the careful mixing process, the next step in the preparation of the composite materials is the casting process. In this regard, the Aerospace and Mechanical Engineering machine shop at the University of Oklahoma was utilized to machine the necessary molds. An aluminum mold was machined to produce four rectangular cavities, measuring 5.25x2.25 inches in total, with 3 of them being 2mm deep and the other 0.5mm deep, as depicted in the schematic diagram presented in Figure 5. The dimensions of the molds were carefully chosen to enable the production of multiple sample types from a single batch of material.

To begin the casting process, mold release agent is sprayed into the mold and allowed to dry for 5 minutes. The material is then scooped into the mold and evenly spread inside the cavities to ensure that it reaches all corners with limited voids. Careful attention is required in this step to ensure that the material is evenly distributed with no air bubbles trapped inside the material. Once the cavity has been filled with the material, another piece of aluminum is used to scrape across the top of the mold, producing a consistent thickness for all the samples. The scraping process is critical to the overall quality of the samples produced and must be carried out meticulously to ensure the material is spread evenly. The final result of the casting process can

be seen in Figure 6, where the result is uniform and high-quality samples needed for accurate and precise testing in the later on.

Figure 5: Aluminum molds with no material

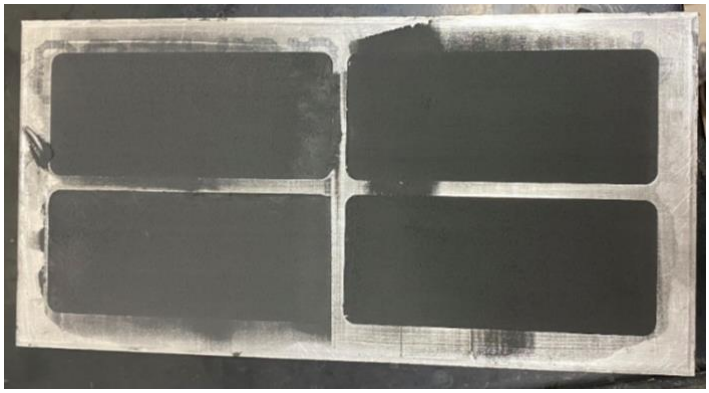

Figure 6: Aluminum molds filled with material

2.4: Overcoming Casting Implications

When casting high loadings of GmB, a challenge was encountered with a curling effect observed during the process of scraping the top surface of the molds. This phenomenon is drawn in Figure

7 and involves the material curling out of the mold as the scraper moves across its surface. There were several different methods attempted to eliminate this problem.

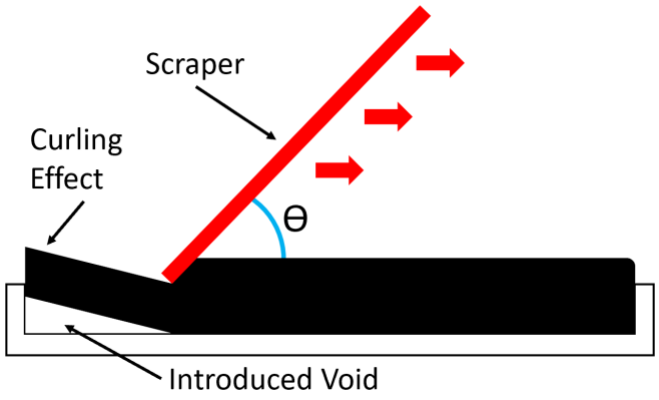

Figure 7: Material Curling Effect

Initially, a thinner piece of metal was sharpened to act as a knife and slice the top off the material. However, this approach did not produce the desired result, as the same curling effect was still observed. Next, a roller was utilized as an alternative method to flatten the material into the molds, similar to the use of a rolling pin in baking. Unfortunately, this technique proved to be unsuccessful, as the material adhered to the roller instead of remaining within the molds, even with mold release applied to the roller's surface.

The next approach involved manually pressing the material into the molds and smoothing the top surface by hand. Nevertheless, this method yielded variable thicknesses among the samples,

which was not acceptable during the testing phase. It was then evident that a more effective solution was necessary to address this problem.

Finally, a scraper made of a thicker piece of metal than the initial attempt was employed. The thick piece of aluminum pushed the material into the mold rather than cutting the top of the material off similar to the thin scraper design. This solution proved to be successful and effectively eliminated the curling effect of the material outside of the mold.

2.5: Curing and Cutting Samples

Upon completion of the casting process, the molds were carefully transferred to an oven and subjected to a temperature of 150°C for a duration of 1.5 hours. This ensured that the samples were fully cured and gave proper results during the testing phase. Once the curing process was completed, the molds were allowed to cool down to ambient temperature before the samples were removed. The use of a mold release agent before casting facilitated the easy and gentle removal of the samples, minimizing the likelihood of any undesired tearing or ripping of the material.

In order to obtain test samples, a set of dies was used for various tests. For instance, a steel ASTM D412-16D standard die was machined to cut dogbone shaped samples for tensile testing.

This standardized method was applied to ensure consistency and accuracy in the tensile strength testing process. In addition, a FDM 3D-printed die was utilized to cut rectangular samples for density and cyclic resistance testing. Finally, a circular die with a diameter of 1/2 inch was used to create samples suitable for thermal diffusivity testing. The tensile and resistance sample shapes were cut from the 2mm thick material while the samples used in thermal diffusivity testing were 0.5mm thick. These samples had to be thinner than the ASTM standard 2mm due to the machine used to measure thermal diffusivity. All the dies used can be seen in Figure 8.

Figure 8: Sample cutting dies

2.6: Electrode attachment

During the course of resistivity testing, it became apparent that an additional critical step was required in order to obtain accurate results. Conductive leads needed to be securely attached to

the samples to ensure the connection of a resistance meter. Initially, copper tape was simply adhered to the back of the sample, as depicted in Figure 9. However, this approach proved to be suboptimal, as the weak adhesive on the copper tape resulted in a high level of contact resistance, leading to unreliable readings during resistivity tests.

Figure 9: Sample with copper tape attached

To address this issue, a conductive silver epoxy was utilized to secure copper strips to the sample. This two-part conductive silver epoxy can be observed in Figure 10, and its implementation significantly reduced the contact resistance between the copper leads and the sample. Moreover, this approach yielded more stable and accurate results. Images of the samples with the conductive silver epoxy and copper strips can be found in Figure 11Figure 11 and Figure 12Figure 11. It was imperative to ensure that the conductive silver epoxy was applied smoothly and completely covered the copper strips to avoid any inconsistencies or errors in the testing process.

The application of a conductive silver epoxy to secure copper strips to the samples represents an essential step in the resistivity testing process. This approach, as compared to the use of copper tape, substantially reduces the contact resistance between the copper leads and the sample, resulting in more accurate and stable test results.

Figure 10: Silver conductive epoxy

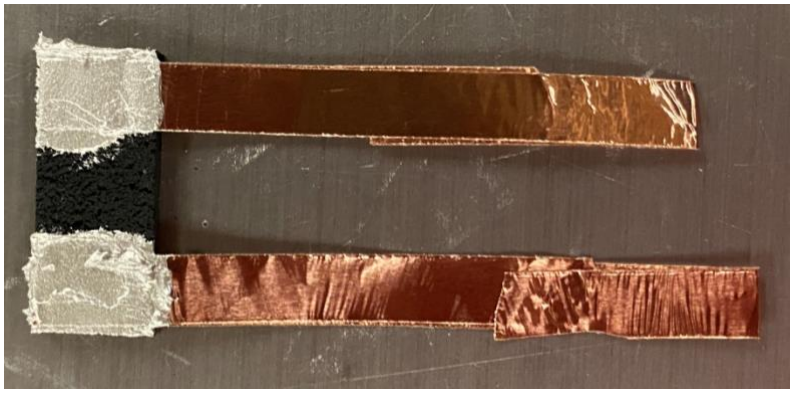

Figure 11: Rectangular samples with epoxied copper electrodes

Figure 12: Dogbone samples with epoxied copper electrodes

Chapter 3: Testing Procedure and Setup

3.1: Testing Purpose

The purpose of the testing phase is to determine various material properties of the composite material. These properties include density, tensile strength, resistivity, thermal conductivity, and lastly thermal effects on resistivity. To discover these properties different types of tests and

experiments need to be conducted. Creating known volume samples and measuring their mass allows for calculation of the material density. Using tensile testing machine, the stress strain curves can be found to determine the material's tensile properties. Utilizing a resistance meter, the resistance of the sample can be measured under different conditions to determine the resistive behavior. Thermal properties can be found with specialized machines designed to accurately and precisely measure thermal conductivity. Physical characteristics can be found be using high powered optical microscopy to visualizes the structures within the composite. All these testing procedures and testing machines will be discussed in greater detail in this chapter.

3.2: Density Testing

The determination of density is a crucial aspect in the characterization and evaluation of various materials, as it plays a significant role in predicting their physical properties and behavior. In this study, density tests were performed to measure the mass of the samples in relation to their volume, enabling the calculation of their density. To ensure accurate and consistent sample preparation, a 3D printed square was utilized to cut rectangles of a uniform size and shape, as depicted in Figure 13. Dimensional measurements were conducted on each sample using a digital caliper with an accuracy of 0.01mm, enabling the precise determination of the width, length, and thickness. Subsequently, each sample was weighed on a highly sensitive scale, such as the Hioki RM 3545 as shown in Figure 14, to determine its mass. The density of each sample was then calculated using the mass and dimensional data, in accordance with the well-established formula

seen below. A total of seven samples were tested for each composite composition, and the results were averaged to determine the average density of the composite material. This meticulous approach to the density testing process ensures the reliability and accuracy of the data obtained.

Figure 13: 3D Printed rectangular die

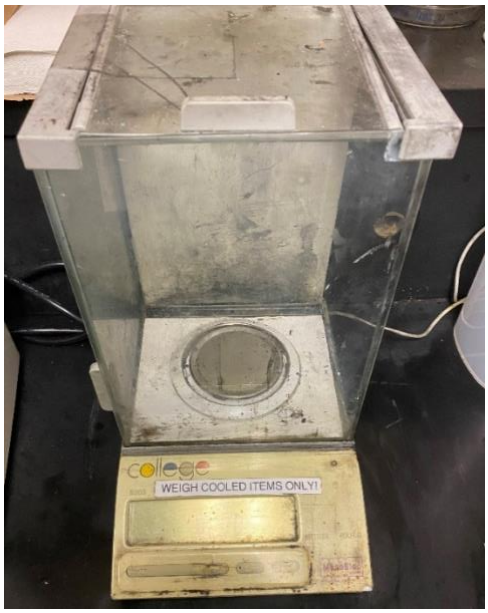

Figure 14: Scale

$$Density = \frac{mass}{volume} = \frac{mass}{width * length * thickness}$$

Equation 1: Formula used for density calculations

As part of this research study, a critical aspect of the investigation involves comparing the measured densities of the different composite compositions to their corresponding theoretical densities. The theoretical density of a material represents the density that it would possess if it were perfectly formed, with no internal voids or defects. This can be used to discover the integrity of the samples since it was a common problem that GmBs were crushed during the mixing procedure, thus significantly increasing the actual density. To determine the theoretical density of each composite, the density of PDMS, CNT, and GmB were found independently. These measurements were then combined, using the percentages of the composite compositions, to determine the theoretical densities of the different composite materials, as per Equation 2. The theoretical densities, therefore, provide a fundamental basis for comparing the measured densities of the composite compositions, offering insight into the extent to which the samples deviate from their idealized forms. By conducting a comparison between the measured and theoretical densities, valuable insights can be gained into the quality and properties of the composite materials being studied. The density comparison was the first test completed to ensure the samples produced accurate results in the remaining tests.

$$Theoretical\ Density = \frac{100}{\frac{PDMS\ \%}{PDMS\ Density} + \frac{CNT\ \%}{CNT\ Density} + \frac{GmB\ \%}{GmB\ Density}}$$

Equation 2: Formula used to calculate theoretical density

3.3: Tensile tests until fracture

In order to gain a comprehensive understanding of the mechanical properties of the composite materials under investigation, dogbone samples that were created earlier were subjected to tensile testing. The Instron 5969 tensile testing machine, which is widely recognized for its high precision and accuracy, was utilized for this purpose, as depicted in Figure 15. The aim of these tests was to generate stress-strain curves that would allow the determination of maximum stress and strains, as well as Young's modulus of the composite materials. To ensure consistency and repeatability, each sample was securely placed in the jaws of the machine, as illustrated in Figure 16, before initiating the testing procedure. The machine was then programmed to pull the sample apart at a constant rate of 2mm/min, while simultaneously taking load and extension measurements. These measurements were critical for calculating the stress and strain experienced by the samples at different stages of the testing process, thus enabling the generation of accurate stress-strain curves. These curves provide valuable insight into the behavior of the composite materials under tensile loading conditions and allow for the determination of fundamental mechanical properties, such as the ultimate tensile strength, strain at failure, and Young's modulus. Overall, the tensile testing procedure is a critical step in understanding the mechanical properties of composite materials, and the use of precise and reliable testing equipment, such as the Instron 5969, is essential for achieving meaningful and accurate results.

Figure 15: Instron 5969 Tensile Testing Machine

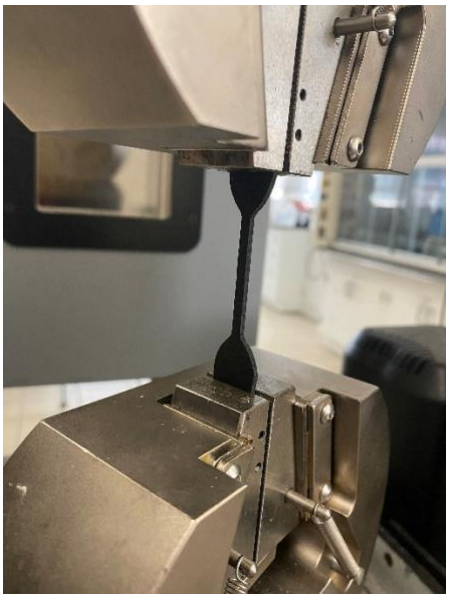

Figure 16: Dogbone sample in tensile testing machine

3.4: Resistivity tensile testing preparation

One critical aspect of the resistance testing procedure was to ensure that the samples were adequately isolated from their surroundings before conducting tensile testing in the Instron machine. In order to achieve accurate resistance measurements during the testing process, it was necessary to prevent any external factors from interfering with the results. However, during the insertion of the samples into the metal jaws of the Instron machine, it was discovered that the resistance remained unchanged throughout the tensile test, contrary to expectations. It was anticipated that the resistance would experience a significant change as a result of the tensile forces acting on the sample. After careful investigation, it was determined that the resistance meter was measuring the resistance of the Instron machine rather than the sample being tested. This phenomenon was caused by the conductive path that was created through the Instron

machine as a result of the silver epoxy making contact with the metal jaws of the machine. This conductive path allowed the current to flow through the machine frame rather than the sample, as the resistance of the sample was significantly higher than the resistance through the jaws and machine frame. This phenomenon, which is depicted in Figure 17, illustrates the importance of conducting a thorough isolation procedure to ensure that the resistance measurements taken during tensile testing are accurate and meaningful.

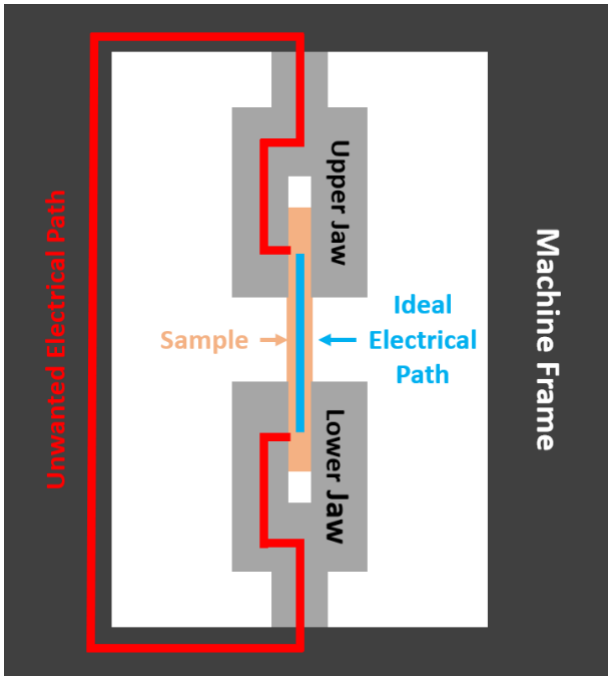

Figure 17: Electrical path possibilities of the resistance meter

To overcome the challenge of measuring the resistivity of the sample instead of measuring the resistance of the Instron machine, it was necessary to establish a non-conductive isolation

between the sample and the machine jaws. To achieve this, several methods were considered and tested. The first approach, seen in Figure 18, was to apply a layer of paper tape to the jaws, which proved effective in isolating the sample and allowing for resistance measurements to be taken. However, this method had its limitations. The stiffness and strength of the silver epoxy applied to the sample meant that over time, the tape would eventually tear, making direct contact between the sample and the jaws possible again. Additionally, at higher strains, the sample would slip as the tape covered the rough texture that was designed to increase friction on the sample. Furthermore, applying the tape to the jaws proved challenging due to the limited space within the jaws, making it difficult to achieve an even and thorough covering of the tape, which could not be replicated accurately when replacing the tape.

Figure 18: Paper tape applied to the metal jaws of the Instron machine

To find a more viable solution, a design for plastic covers was created using Autodesk Fusion 360. The design was optimized to fit the jaw dimensions of the Instron tensile testing machine accurately. This design is seen in Figure 19. The plastic covers provide a stronger and thicker barrier between the sample and metal jaws. Due to their durability and strength, they will not tear like the paper tape method, and the rough texture on the surface allows for a better grip on the sample. In addition, the design uses the existing pins on the upper and lower jaws to hold the

plastic covers in place, thereby eliminating the need for tape or glue. The result is a reliable and repeatable solution that provides consistent resistance measurements throughout the tensile test.

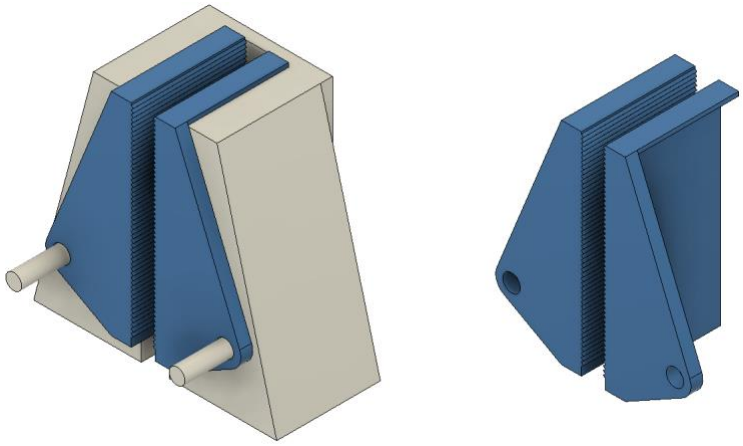

Figure 19: CAD design of non-conductive plastic jaws

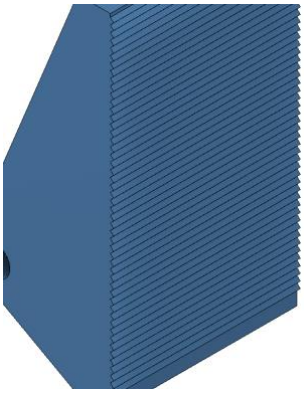

Figure 20: Close view of textured surface to increase grip

To design the plastic jaw covers, precise measurements were taken during the partial disassembly of the machine to ensure that the covers fit the jaws accurately. These measurements were then used to create a 3D model of the covers. The model was optimized to fit the jaw

dimensions perfectly and provide a rough surface for better grip on the sample. The final product was then 3D printed, and several tests were performed to ensure that there was no slipping between the sample and the plastic cover or between the metal jaws and plastic covers. The final 3D printed covers can be seen in Figure 21.

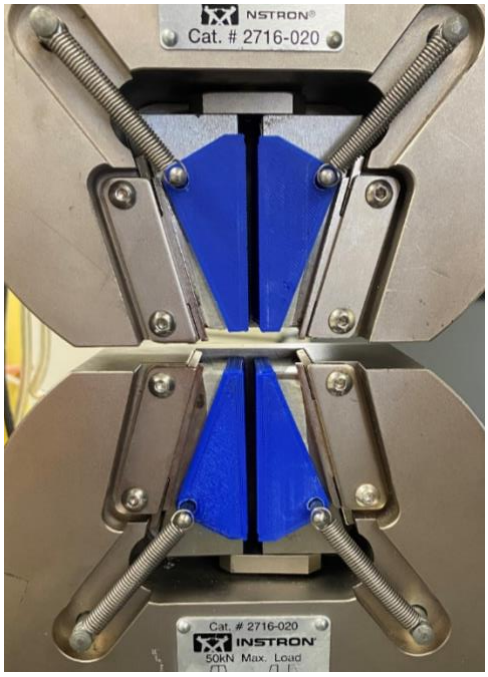

Figure 21: Installed non-conductive plastic jaws on Instron machine

The design and implementation of plastic covers for the Instron tensile testing machine's jaws provided a reliable and repeatable solution for isolating the samples from the machine's metal jaws, thus eliminating the inaccuracies in the resistance measurements. This solution not only

eliminates the need for unreliable paper tape but also provides a better grip on the sample, making the tests more consistent and accurate. The design process was a meticulous and precise task, and the final product has proven to be an effective solution for the resistance measurement challenges encountered during the tensile testing.

3.5: Resistivity tensile tests until fracture

In addition to conducting tensile tests, simultaneous resistivity tests were carried out to collect data on the electrical properties of the composite materials. To ensure accurate and reliable measurements, a resistance meter was utilized, specifically the Hioki RM 3545, as it is capable of high-speed sampling at a rate of 450Hz and can record data automatically into a CSV file. To connect the resistance meter to the samples, clips were attached to the copper leads on the sample, as shown in the Figure 22. This setup allowed for the continuous monitoring of the resistance of the sample during the tensile test. By collecting data on both the mechanical and electrical properties of the samples simultaneously, a comprehensive understanding of the behavior of the composite materials under different stresses and strains could be achieved.

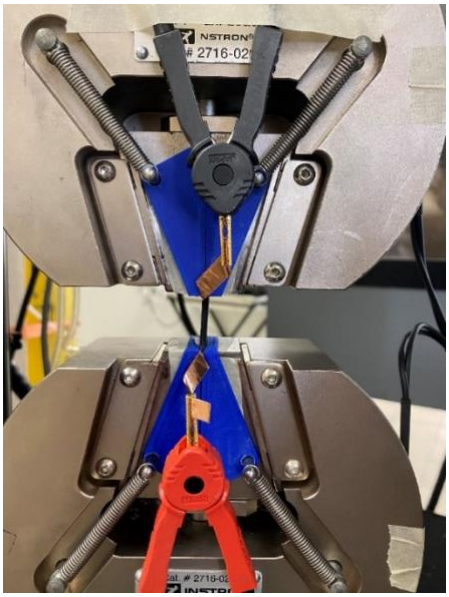

Figure 22: Resistance meter connected to copper electrodes

Figure 23: Reading on the resistance meter once connected to the sample

3.6: Extended Length Cyclic Resistance Tests

Following the successful completion of the fracture tensile tests, cyclic tensile resistance tests were conducted. The test setup for this experiment was similar to that of the fracture resistance tests, as the same Instron 5969 tensile machine and Hioki RM3545 resistance meter were utilized. Rectangular samples, which had been previously prepared with silver-epoxied copper leads, were clamped into the Instron, and connected to the resistance meter.

In order to determine the appropriate parameters for the resistance cyclic tests, the maximum strain data gathered during the initial tensile tests was used to determine new strain values. Specifically, 75% of the maximum strain value was calculated for each composite composition individually. With the newly calculated value, the Instron was then programmed to perform 250 cyclic loads on the sample to the 75% maximum strain at a rate of 25% strain per minute, while the resistance meter simultaneously recorded resistance data.

Once the cycles were completed, the resistance data was processed to align both the tensile and resistance data sets together. This allowed for a comprehensive analysis of the composite material's performance characteristics under varying loads and strain levels.

3.7: Variable Strain Cyclic Resistance tests

After conducting the resistance cyclic tests as described earlier, the next experiment involved subjecting the sample to a series of 30 cycle tests at different strain amounts. To accomplish this, the sample was left in the tensile machine and connected to the resistance meter, allowing for simultaneous strain and resistance data collection.

Similar to the previous test, the appropriate strain values for the cyclic tests were found as a percentage of the max strain the composite could withstand. The values for 2, 5, 10, 15, 25, and 50% max strain values were identified for each composite composition. These values were then used to program the tensile machine to stretch the sample to 2% max strain for 30 cycles before moving on to 5% max strain and so on, until all six strain values had been tested.

Throughout the testing process, the resistance meter was collecting data to measure the resistance change of the sample compared to the strain value. By subjecting the sample to multiple strain amounts and collecting corresponding resistance data, valuable insight into the material properties and performance of the composite material were discovered.

3.8: Temperature Influence on Resistance tests

To determine the thermos-resistance properties of the composites, a series of tests were conducted to measure the resistance of the specimens in different temperature ranges. To do this, rectangular samples identical to those employed in cyclic testing were prepared.

The Hioki RM3545 resistance meter was used to obtain the resistance data. The samples were placed inside a Cole-Parmer furnace, as seen in Figure 24, which features a vent hole on the top side where the resistance meter wires were fed through. Notably, the Hioki RM3545 meter includes a Z2001 temperature sensor, which allowed the meter to data log the temperature inside the furnace.

The experimental setup involved programming the Coleman Furnace to incrementally increase the temperature from 30°C to 90°C by 10°C steps. Once the target temperature was reached, the samples were left to soak for 5 minutes to ensure stabilization before increasing the temperature further. After the soaking period at 90°C was completed, the samples were then left to cool to room temperature. During this process, the resistance meter was continuously logging resistance data.

In particular, the resistance values were recorded at the end of each soaking period to be plotted later on. The resulting dataset will serve as a basis for the analysis and interpretation of the composite material's resistance behavior under varying temperature conditions.

Figure 24: Furnace samples were placed into

3.9: Thermal Diffusivity tests

To characterize more thermal properties of composite materials, an experimental investigation was carried out to determine the thermal diffusivity of the materials. To complete these tests, a collaboration with Dr. Jivtesh Garg's Micro/Nano Heat Transfer Laboratory at the University of Oklahoma was needed. To carry out the testing, a Laser Flash Analysis (LFA) machine was

used, which is a widely accepted method for measuring thermal diffusivity. Specifically, the Netzsch HyperFlash 467 was used, seen in Figure 25, which is known for its high precision and accuracy. The experiment involved using quarter inch circular samples that were fabricated earlier, which had a thickness of 0.5mm. It is important to note that the LFA machine operates by using a laser to deliver the energy required for the test. Hence, it is critical that all the energy from the laser is absorbed by the sample with minimal energy reflected. To ensure complete absorption of the laser energy, the samples were coated with a thin layer of graphite, which has high thermal conductivity thus minimal interference with the testing results. The coated samples can be seen in Figure 26.

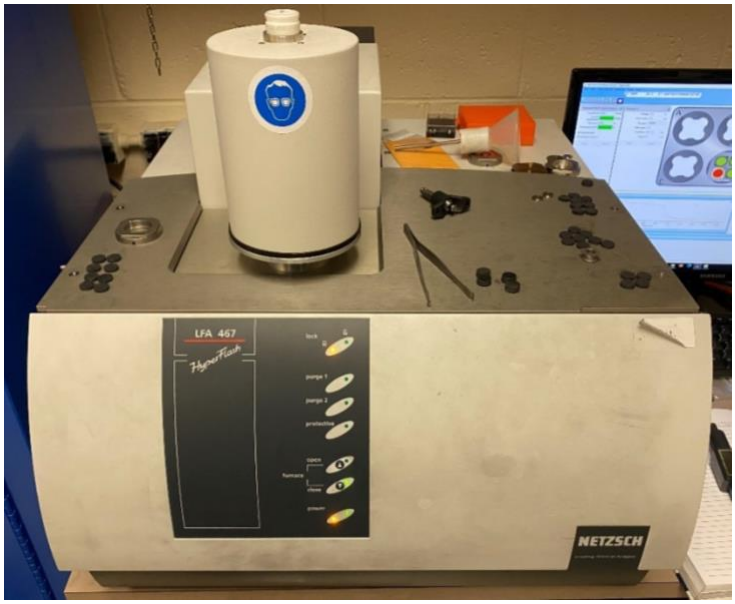

Figure 25: Netzsch HyperFlash 467 machine

Figure 26:Graphite coated samples

In essence, the LFA machine measures the amount of time it takes for an energy source to travel into the bottom of the sample and out of the top side of the sample. In this particular experiment, a laser pulse was sent into the sample from the bottom, and a highly sensitive sensor was utilized to detect when the energy passes through the thickness of the sample. Notably, this process was conducted in a precisely temperature-controlled chamber that was isolated from the outside environment to ensure accurate results. A schematic of the experimental setup can be seen in Figure 27. With the time delay measured from the machine, the thermal diffusivity of the composite material was calculated using the known thickness of the sample with Equation 3.

$$\alpha = 0.1338 * \frac{d^2}{\frac{t}{2}}$$

Equation 3: Thermal diffusivity calculation with time delay

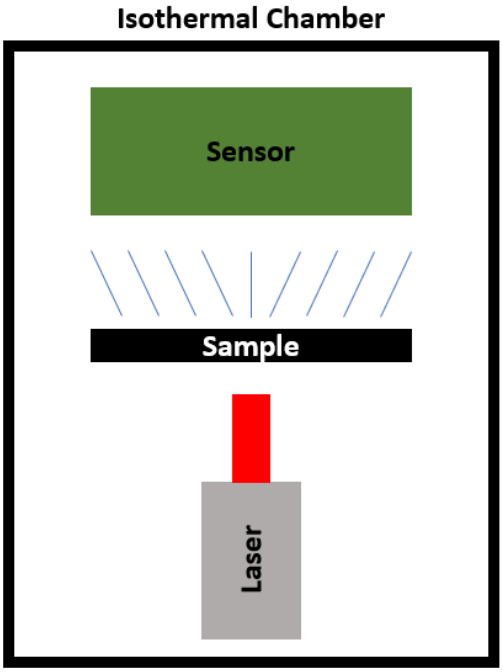

Figure 27: LFA machine theory diagram

Based on the thermal diffusivity results, it is possible to calculate the thermal conductivity of the composite materials by using the specific heat and density values of its individual components. Theoretical specific heat values of the various composites can be determined using a formula that involves the combination of different percentages of additives, as shown in Equation 4. This

method closely resembles the process of calculating theoretical density values, which was previously performed. Theoretical density values will also be utilized to calculate the specific heat of the composite material. Once the theoretical specific heat values have been obtained, they can be used in combination with the theoretical density values to determine the thermal conductivity of the composite material by applying Equation 5.

$$Theoretical\ Specific\ Heat = \frac{100}{\frac{PDMS\ \%}{PDMS\ C_p} + \frac{CNT\ \%}{CNT\ C_p} + \frac{mGB\ \%}{mGB\ C_p}}$$

Equation 4: Formula used to calculate theoretical specific heat

$$k = \alpha \rho C_p$$

Equation 5: Thermal diffusivity to thermal conductivity

3.10: Optical Microscopy

In order to conduct a more in-depth examination of the composite materials, the samples were processed through a microscopic analysis. To carry out this task, the Keyence VHX-7000 optical microscope, seen in Figure 28, that is renowned for its superior resolution and imaging capabilities, was employed. This advanced microscope is equipped to capture images with 4K

resolution and provides zoom capabilities of up to 6000x with 4 switchable lenses, enabling a detailed inspection of even the nano particles within the composites.

Figure 28: Keyence VHX-7000 optical microscope

One common challenge encountered during high-magnification microscopy is the issue of surface roughness, which can cause significant height variation in the sample. When there is height variation, it can be difficult or even impossible to achieve optimal focus throughout the entire image. However, the custom VHX software incorporated in the microscope has the unique capability to detect areas of the image that are in focus and those that are not. With this ability,

the microscope can slowly adjust the focus throughout the image capturing process, then extract the highest quality portions at each focusing level to construct a single image with every aspect of the sample being in focus.

Moreover, the Keyence VHX-7000 microscope has the ability to understand its current zoom level and distance between the lens and sample, enabling it to make dimensionally accurate measurements. Once an image has been captured, the user can draw lines or circles to measure different particles within the composite, making it an invaluable tool for quantitative analysis.

In addition to the advanced focusing technology mentioned earlier, the custom VHX software incorporated in the Keyence VHX-7000 microscope has an additional capability to calculate the depth at which each focused area is located. By using this technology, the microscope can detect surface variations of the sample as the image is slowly focused in. This feature enables the software to generate a 3D view of the surface from the final image captured. This 3D mapping technology is a valuable tool for better understanding the properties of the composites being analyzed and the effects of the casting process. The generated 3D maps allow for a visualization of the surface roughness of the samples in great detail, providing insights into the nature and distribution of the composite particles.

The Keyence VHX-7000 optical microscope also has the ability to move the stage in both the X and Y directions to examine different areas of the sample. With the stitching operation within the VHX software, users can select a 3x3 or 5x5 grid for a larger image to be taken. The sample is then moved in the X and Y directions, and images are captured according to the selected grid size. The VHX software then automatically stitches the 9 or 25 images together into a single, comprehensive image. This unique capability allows for the collection of very large images that contain significantly more data than a single stationary image. The stitched image provides a panoramic view of the sample, providing insights into the overall structure and characteristics of the composite material being analyzed.

To begin looking of the sample, the lens with the lowest magnification is selected and the sample is placed below it. The bottom plate, or stage, is now raised until the sample starts to appear within the image. Using the control panel seen in Figure 29, the sample can then precisely be moved in the Z direction until the image is within focus. The next lens is now selected which increases the magnification of the image and now the fine tune focusing process is done again. This same process is repeated until the desired zoom level is reached.

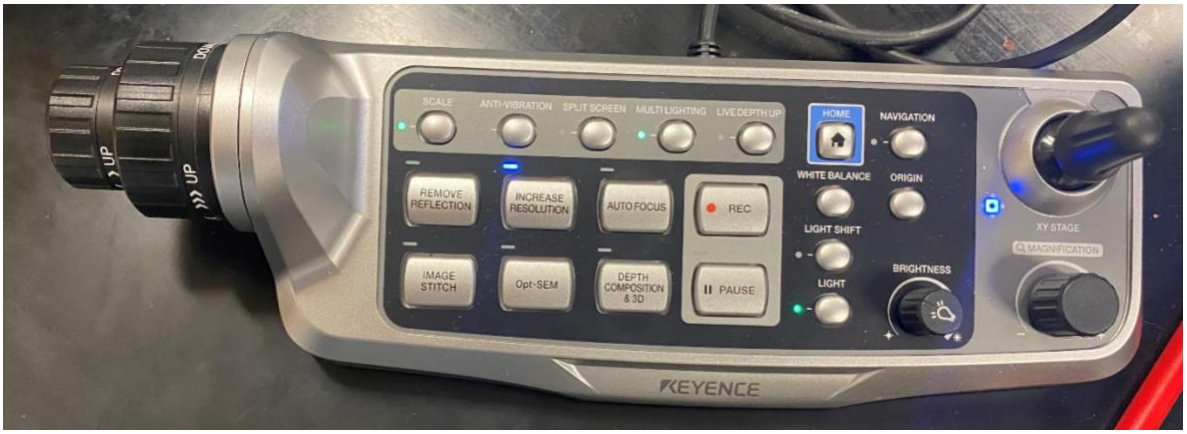

Figure 29: Control panel for microscope

During the tests completed, large, stitched images were taken at multiple different zoom levels as well as 3D views of each sample. For the samples containing GmB, the glass balloons were measured using the measuring feature to determine the average diameter of the spheres.

CHAPTER 4: DISCUSSION AND RESULTS

4.1: Density Results

To begin with the results, the calculated density values will be evaluated. Utilizing the measured density values and theoretical calculated values discussed earlier, the sample's quality can be determined [38]. To calculate the theoretical densities of the various compositions, the individual component densities seen in Table 1 will be used [39-41]. The final calculated theoretical and measured densities can be seen in Table 2 and visualized in Figure 30.

Table 1: Density values for additives in the composites tested

Additive	PDMS	CNT	GmB
Density (g/mm^3)	0.00103	0.0018	0.00013

Table 2: Measured densities and calculated theoretical values

GmB %	0	5	10	15	20
Measured (10^3)	1.027	0.749	0.591	0.493	0.477
Theoretical (10^3)	1.036	0.759	0.599	0.495	0.481
% Difference	0.80	1.39	1.47	0.49	0.88

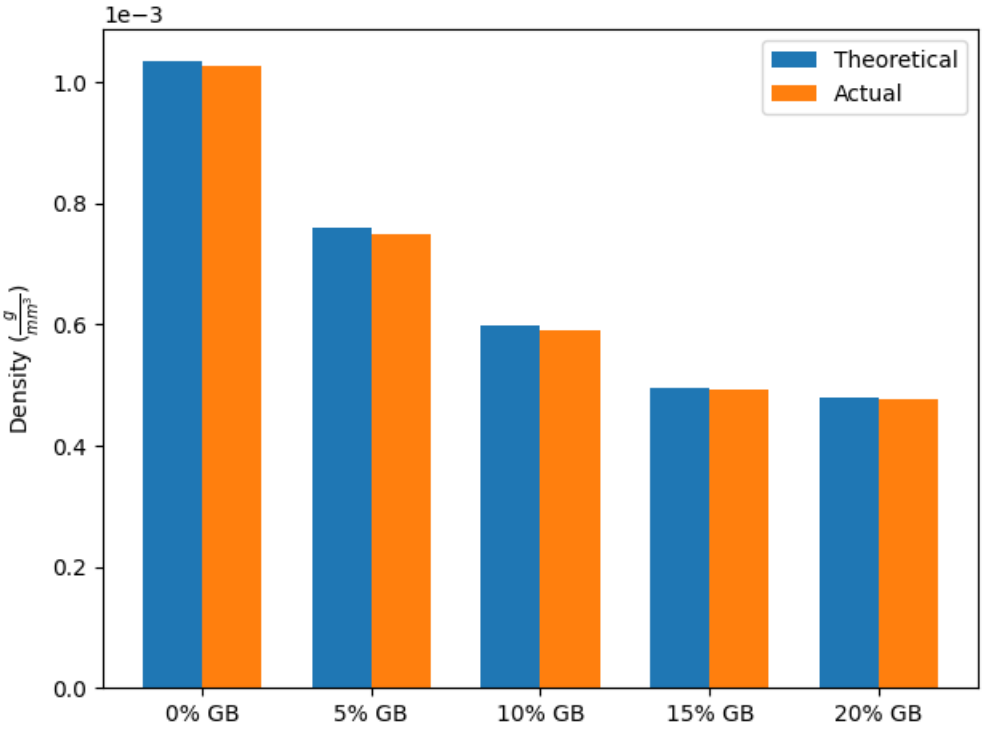

Figure 30: Theoretical and measured density values

From the results it can be determined the samples remained within 1.5% of the ideal density. A unique take away from the results is the measured values were consistently lower than the theoretical value. This phenomenon is most likely caused by internal voids within the material introduced during the mixing or casting processes. The results also proved that no GmBs were crushed during the mixing process since the measured densities would be significantly greater due to the GmB having less volume when broken. It was determined the results of this test guaranteed the integrity of the composites and allowed them to be farther tested.

4.2: Tensile results

Following the tensile tests performed with the Instron 5969, the stress and strain results can be analyzed. The stress strain curves can be generated from the results to determine the max tensile strain, max tensile stress, and Youngs Modulus. The consistent stress strain plots can be seen in Figure 31 depicting the repeatability of results across multiple samples. The small variation within each sample tested shows the acquired results reflect a true and accurate description of the material properties.

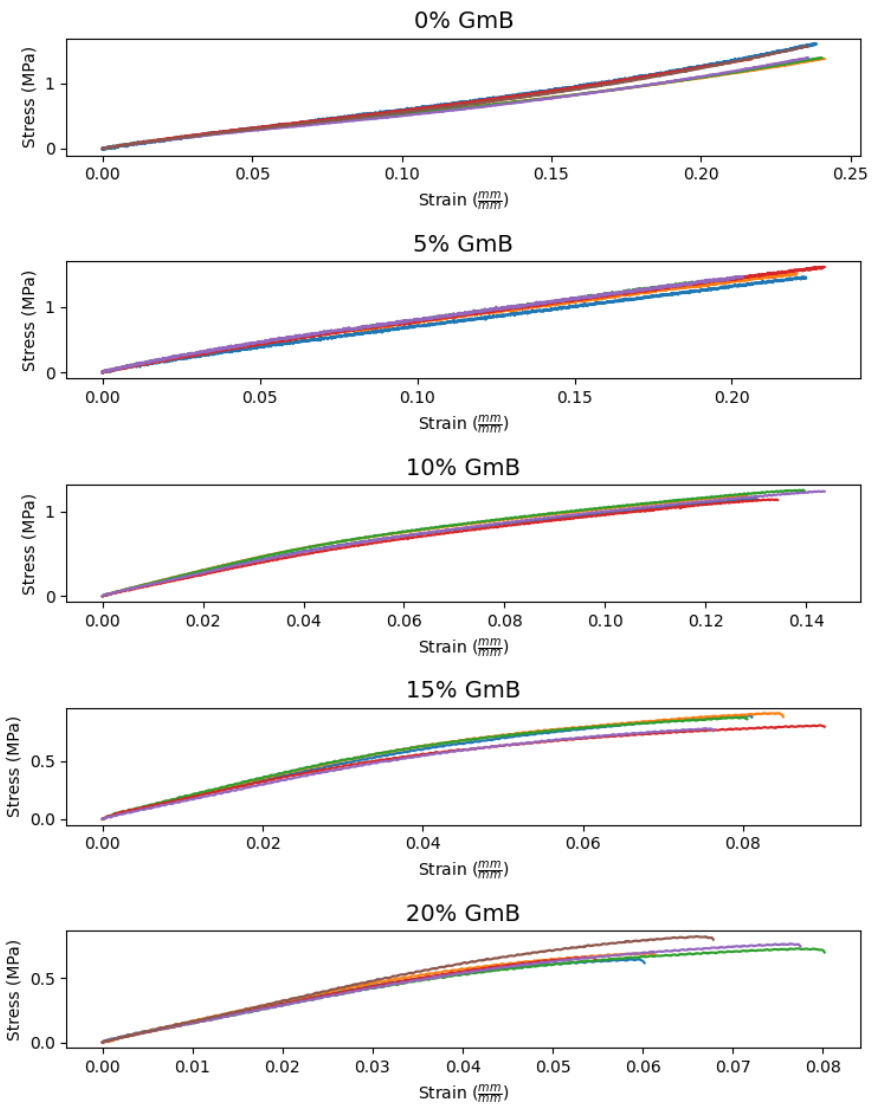

Figure 31: Stress v. strain plots for all compositions

From the stress strain curves the maximum stress can be plotted seen in Figure 32. Similarly, the composite max strain and modulus can be seen in Figure 33 and Figure 34. These plots were

created by taking the average max stress, max strain, and modulus values of 4 samples within each composite composition. The error bars present on the plots represent the standard deviation between the samples.

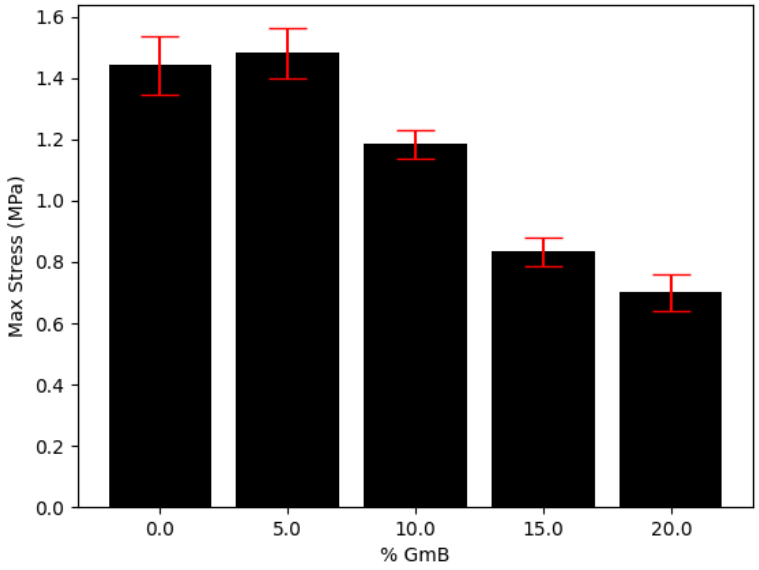

Figure 32: Maximum stress of all compositions

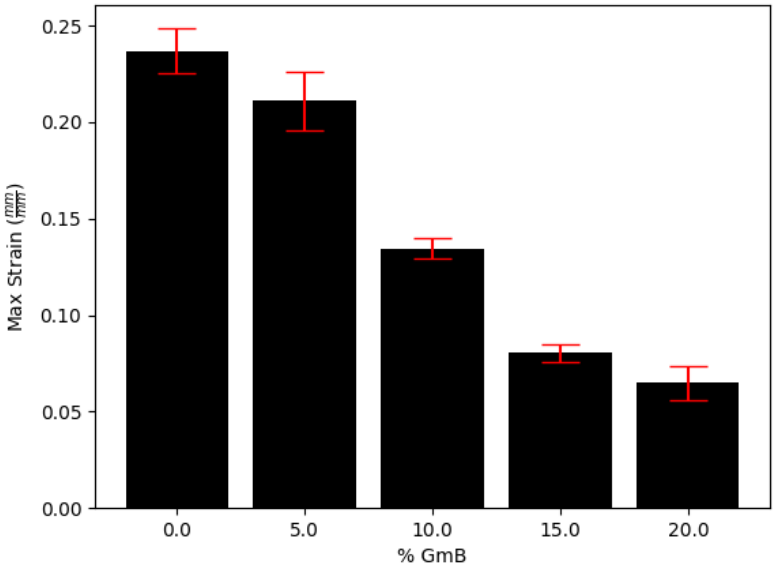

Figure 33: Maximum strain of all compositions

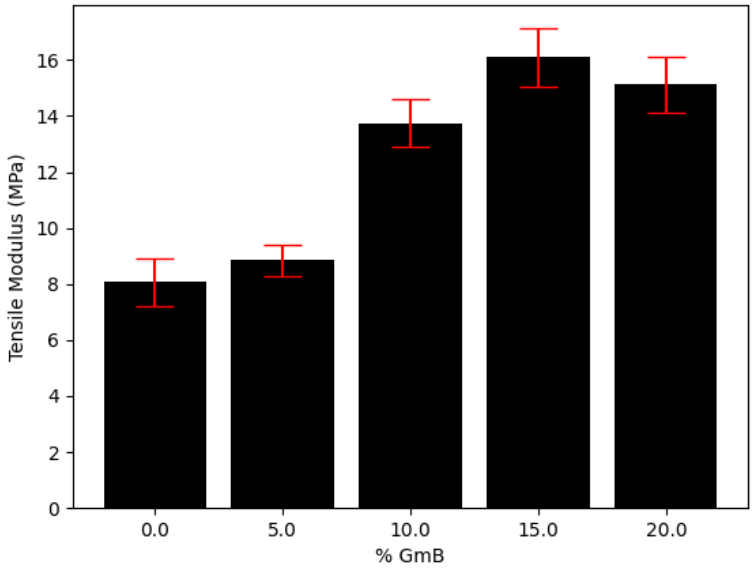

Figure 34: Modulus of all compositions

From these results it can be determined that adding higher loads of GmB to the composite will decrease both the maximum stress and strain the material can withstand but also increase the Youngs modulus.

4.3: Resistance until fracture results

While recording tensile data from the tensile test, resistance data was also being recorded simultaneously. Similar to the stress strain curves, resistance strain curves were generated. All the resistance strain curves can be seen in Figure 35 which display accurate and consistent results from each sample in each composition.

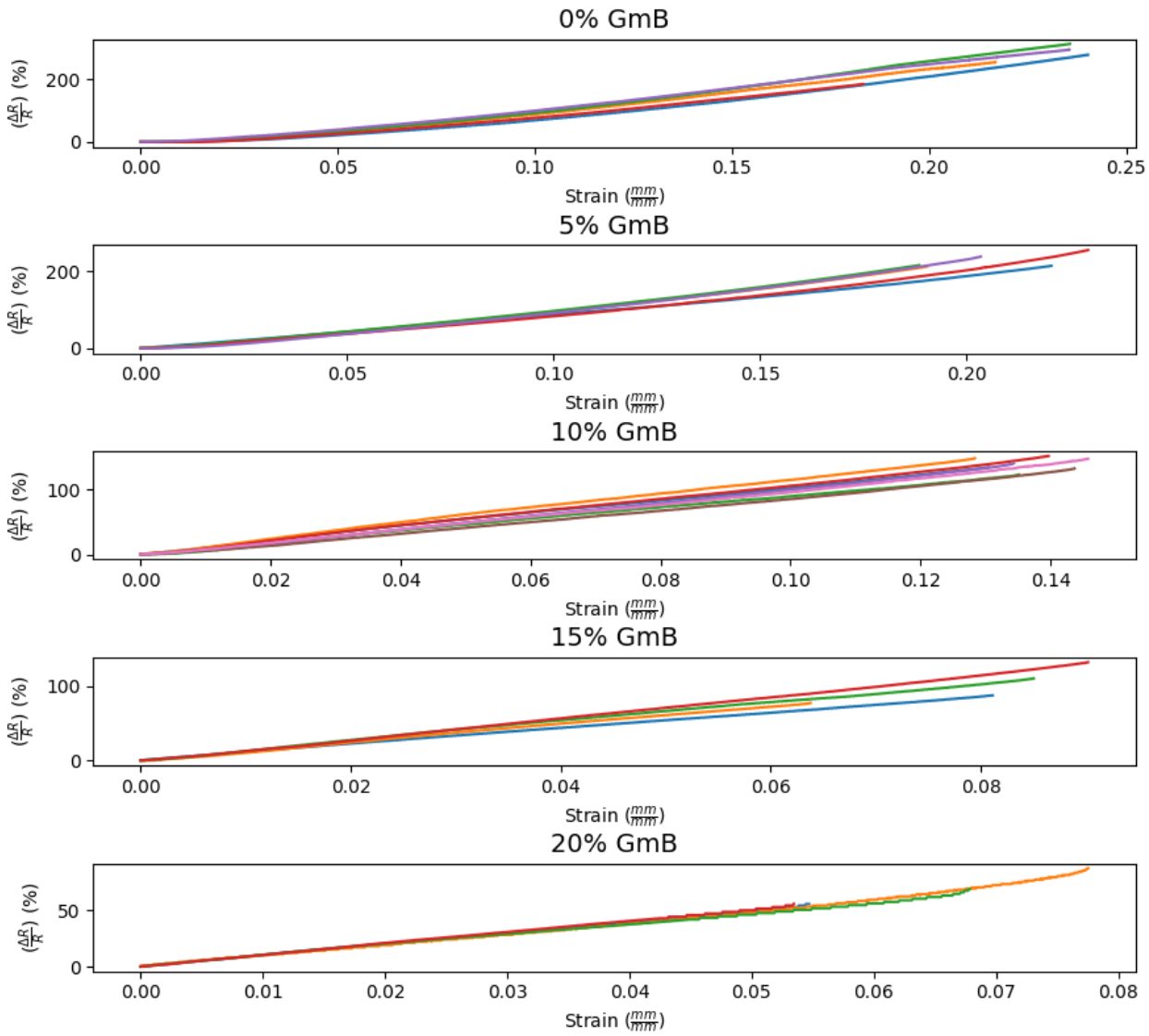

Figure 35: Resistance v. strain for all compositions

As seen in Figure 36, the greatest change in resistance while stretching the sample until fracture was the composition with no GmB. As the loadings of GmB went up, the resistance change value decreased. In reality, this is reasonable since glass is an electrical insulator meaning it does not

conduct electricity easily. The more glass contained within the sample the less conductance thus less resistance change.

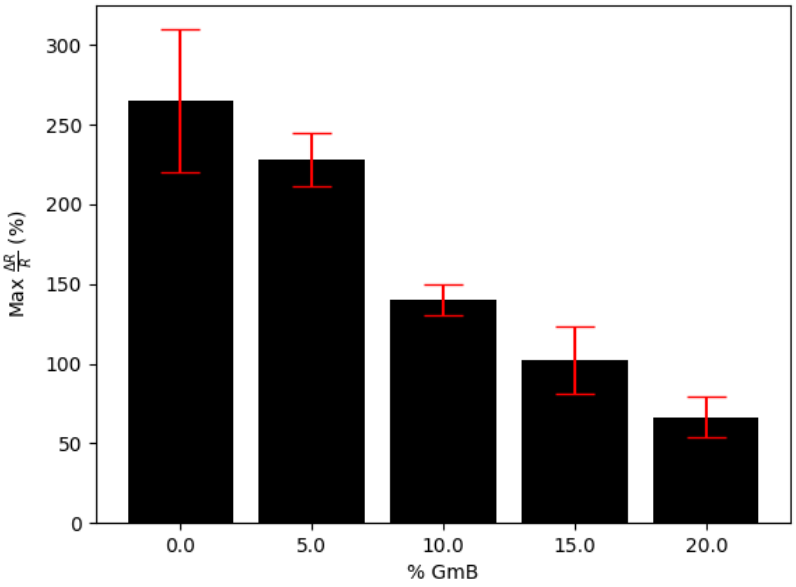

Figure 36: Maximum resistance change for all compositions

Using the same principle of glass electrical insulation, the resistance of the samples should increase with the loading of GmB under no load. As seen in Figure 37, this statement is true since the resistance of the composite steadily increases, then significantly increases with a loading of 20% GmB.

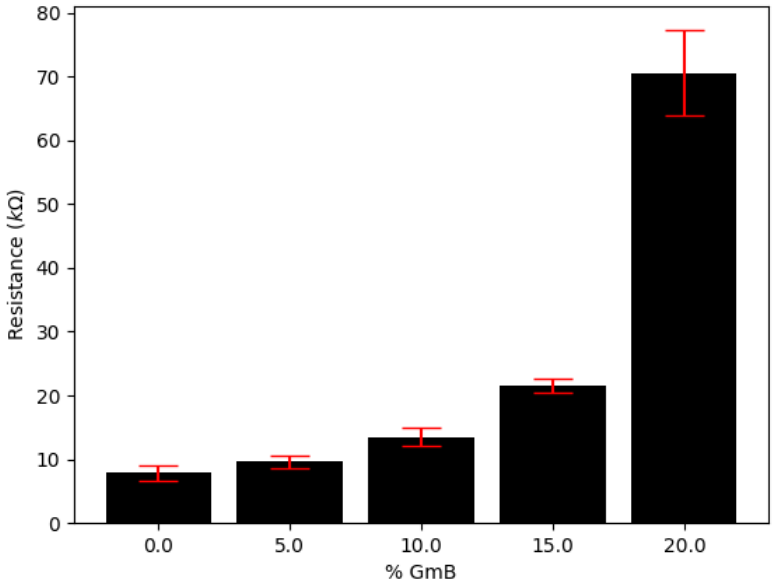

Figure 37: Averaged initial resistance of multiple samples with standard deviation error bars

4.4: Cyclic resistance results

In addition to measuring the resistance of the sample in tensile loading until fracture, the sample was also subjected to cyclic loading. The samples first underwent 250 cycles to prove the repeatability of the resistance measurement values, these results can be seen in Figure 38. The results look as expected, the composite slowly drifts downward until stability is found, then each cyclic gives repeatable resistance measurements. It is worth noting that the lower GmB loadings had a trend of reaching stability in fewer cycles than those with higher loadings.

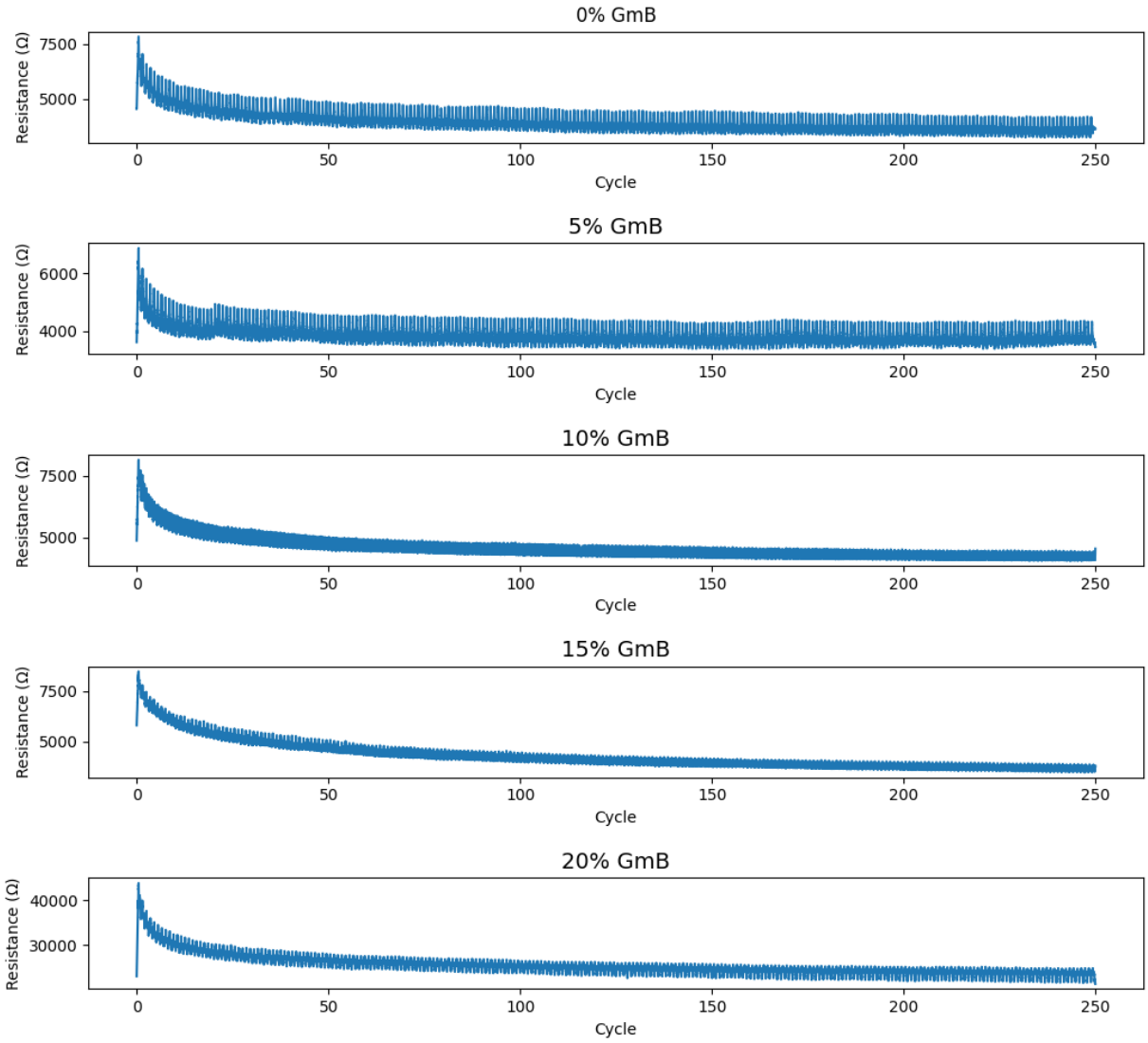

Figure 38: Resistance change v. cycle number for all compositions

In addition to the 250 cycle tests, shorter 30 cycle tests were completed at different strain amounts. These resistance tests were completed to 2, 5, 10, 15, 25, and 50% of the max strain of the composites. The results can be seen in the following figures. It is worth noting that the composite containing a 20% loading of GmB consistently has a resistance change 2-3 times

greater than the other composites. The results from all compositions are all very consistent, allowing for an accurate comparison between all samples.

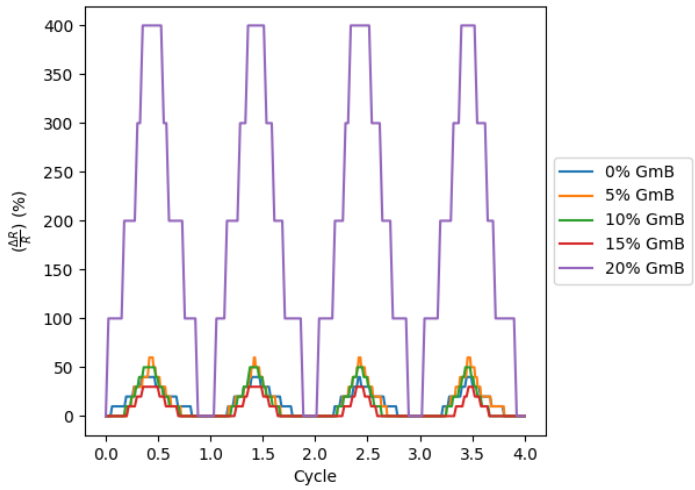

Figure 39: 2% max strain section from 30 cycle test

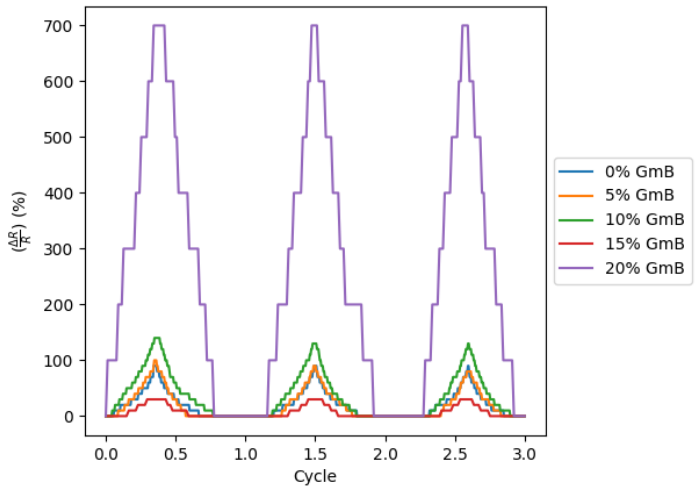

Figure 40: 5% max strain section from 30 cycle test

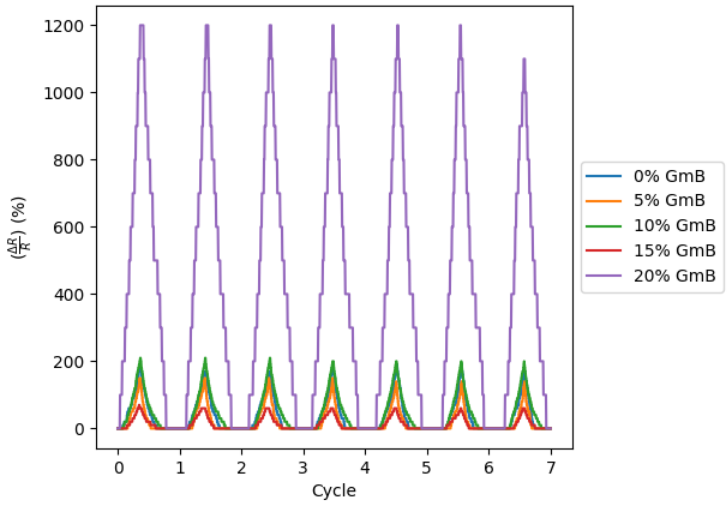

Figure 41: 10% max strain section from 30 cycle test

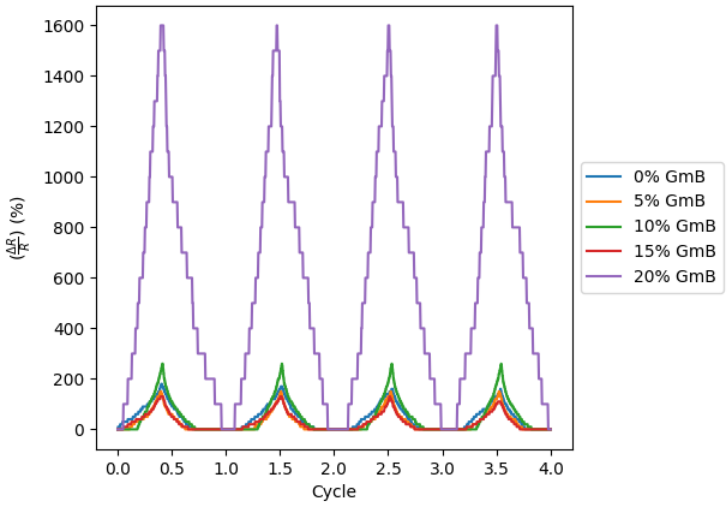

Figure 42: 15% max strain section from 30 cycle test

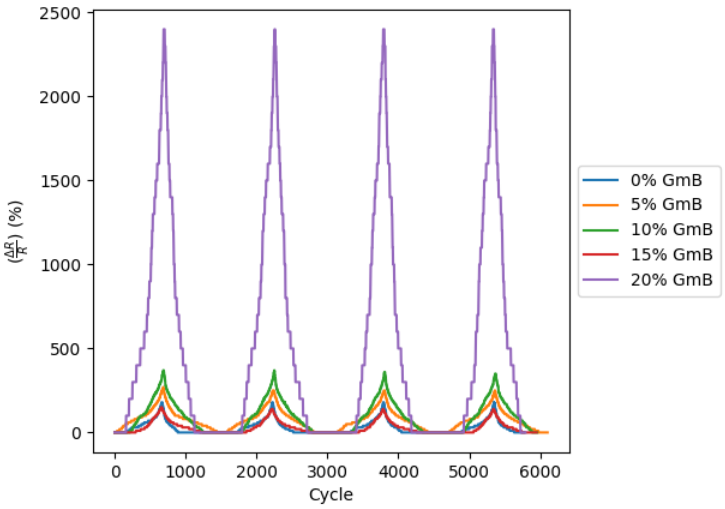

Figure 43: 25% max strain section from 30 cycle test

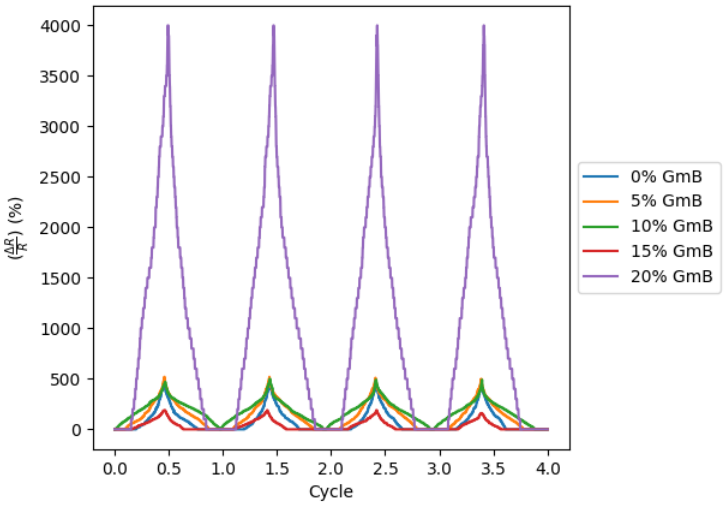

Figure 44: 50% max strain section from 30 cycle test

4.5: Thermal results

Next, the results from the thermal analysis will be discussed. The results from the thermal testing directly measured the thermal diffusivity. Using those results and the specific heat of the individual composite additives, the thermal conductivity can be calculated. For each composition, 4 samples were tested, while the results were averaged and an error bar was generated using the standard deviation. These results are plotted in Figure 45 and Figure 46 respectively. As the loading of GmBs increased, the thermal diffusivity increased while the thermal conductivity decreased. This means heat takes more time to flow through the composite thus making it a better insulator and more resistant to heat. This makes sense since glass is known to be a very good thermal insulator.

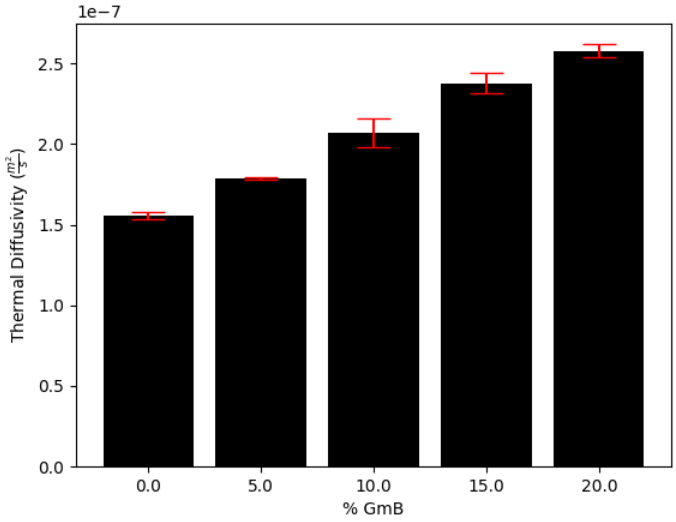

Figure 45: Averaged thermal diffusivity between 4 tested samples

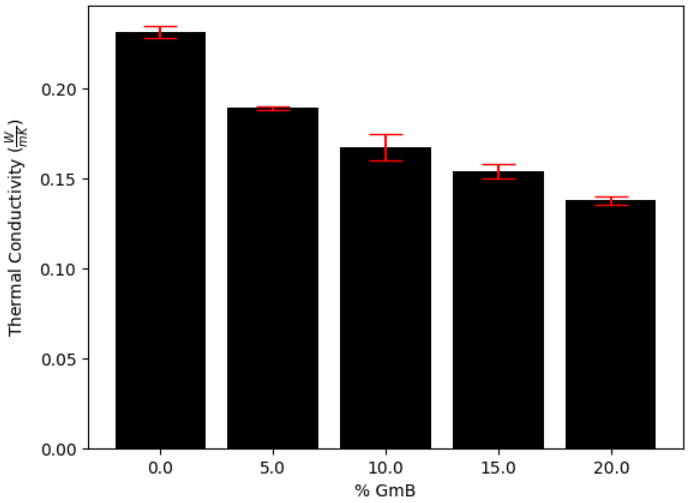

Figure 46: Averaged thermal conductivity between 4 tested samples

The next test preformed uncovered the effects temperature has on the resistance of the samples. As the samples were heated, resistive data was taken and plotted in Figure 47. It was discovered the composition with a 10% loading of GmB gave me the most stable resistance results throughout the entire temperature range. The higher GmB loadings had a dramatic decrease in resistance during the test.

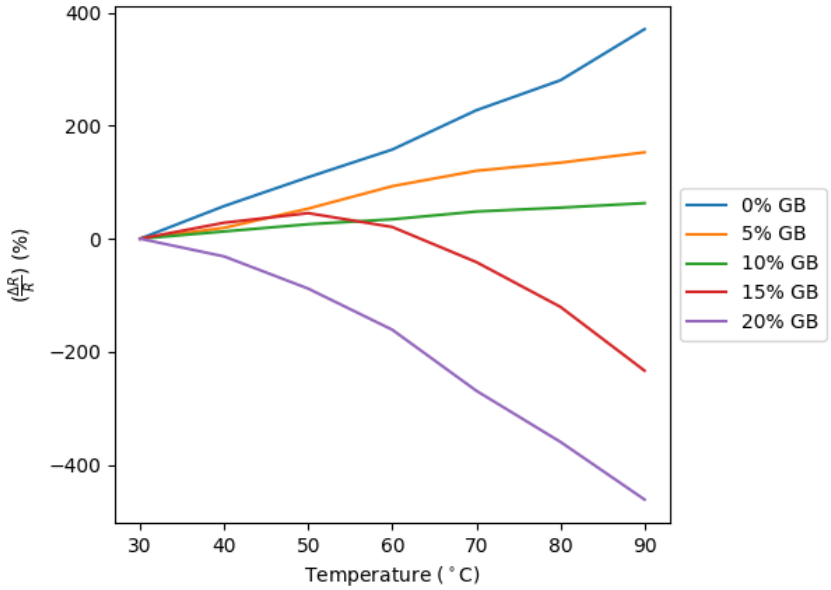

Figure 47: Resistance change of sample at varying temperatures

4.6: Optical microscopy results

To obtain physical images of the composite materials, a high-power optical microscope was used to image the surface of the samples. Using the 400X magnification images, it was determined the GmB had very even and consistent dispersion throughout the sample seen in Figure 48. The reflection of the microscope light on the glass allowed the balloons to be easily visualized. Utilizing the measuring tool the microscope is capable of, it was found the GmBs had largely varying diameters seen in Figure 49, with an average diameter being 13.20µm.

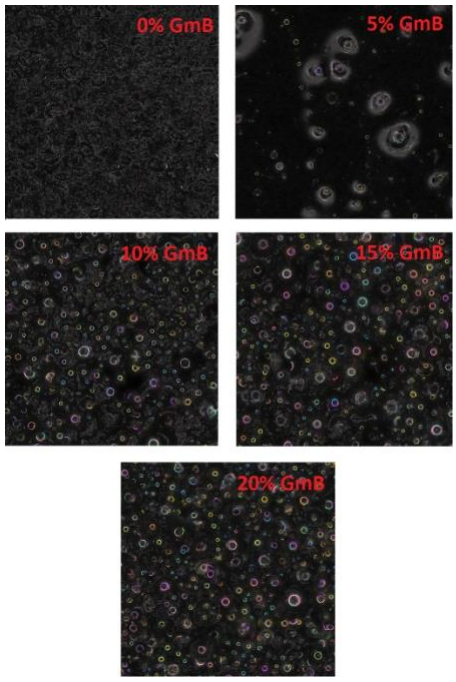

Figure 48: 400X zoom of all compositions

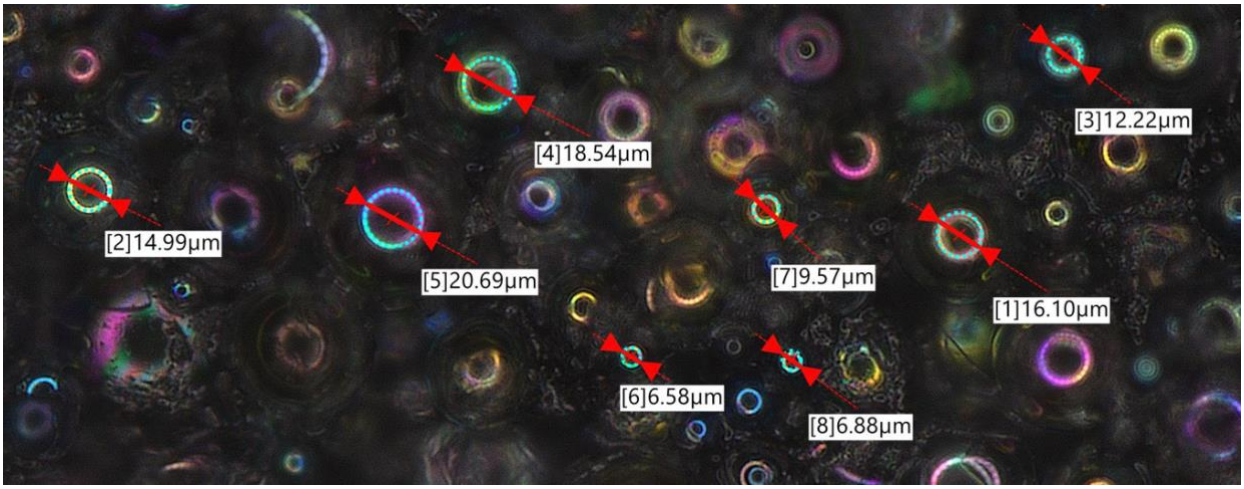

Figure 49: Measured GmB diameters

Zooming in farther to 2500X, the microscope was able to image the CNTs within the composite. The images allow for the level of CNT dispersion to be visualized and to determine the amount of CNT agglomerations. In Figure 50, the small white lines are the CNTs while the large colorful areas are the GmB. It can be seen that the CNTs are well dispersed with minimal agglomeration which can be difficult to overcome when using centrifugal mixing methods. Those composites with GmB made visualizing the CNTs more difficult since the glass reflects light back into the lens causing some areas to be blurry.

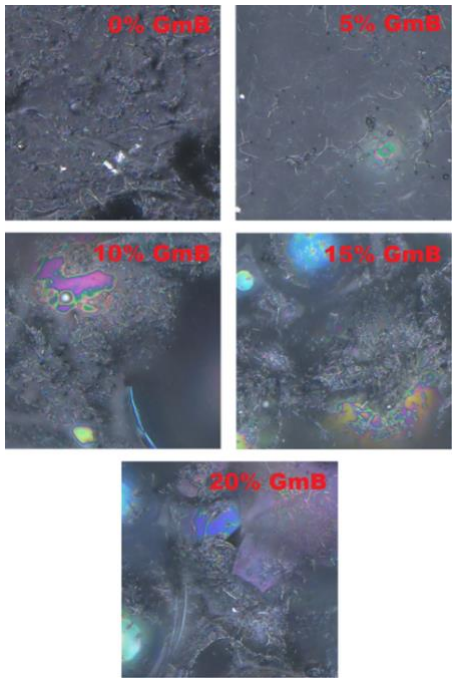

Figure 50: 2500X zoom of all compositions

CHAPTER 5: CONCLUSIONS AND FUTURE WORK

Developing nano CNT and GmB nano-composites have shown to be a viable way to produce highly flexible and heat resistant sensors. In order to create these sensors, a great deal of research was conducted to determine possible additives that could express these behaviors once combined into a composite material. It was determined that multiple different composite compositions needed to be investigated to determine the effects of different weight percentages of GmBs, starting at 0% and working to 20% in 5% increments. After the compositions were established, a careful and consistent sample preparation method was established. The mixing and casting process was an intricate process to ensure no GmBs were damaged or crushed while also ensuring proper dispersion of CNTs and GmB. Since this material is designed to be a sensor, a strong and reliable method needed to be chosen to attach copper electrodes to the sample. To do this, conductive silver epoxy was utilized to guarantee a low resistance connection between the copper and the sample. After all the samples were produced, it was now time to begin testing the samples to determine various material properties. The first test preformed was to measure the density of the material and compare it to the ideal theoretical density. It was found that the density for all compositions measured within 2% of the theoretical density showing that GmB were not crushed during the production of the sample and that the material integrity was great enough to continue testing. Next, using a tensile testing machine, the sample was pulled until fracture while simultaneously measuring resistance. This test allowed for the max stress, strain, and resistance as well as the modulus to be determined. It was shown that the composite with 0-

5% GmB was 2-3 times stronger than the other compositions. However, it was discovered that the composition with 20% GmB had the largest change in resistance. To farther investigate the resistive behavior of the materials, the samples were subjected to a series of cyclic tensile tests while resistance was being measured. The first cyclic test consisted of bringing the sample to 75% of the maximum strain 250 times. From this test it was found that all compositions consistently and repeatedly measured the same resistance change while having very little drifting in the data. After the first cyclic tests were completed, the sample then underwent a series of 30 cycle tests, bringing the sample to 2, 5, 10, 15, 25, and 50% maximum strain. This test allowed the repeatability and sensitivity of the sensor to be visualized while it was discovered the 20% GmB composition again had a significantly higher resistance change at all strain values. To determine the thermal property effects of the GmBs, the samples were placed in an LFA machine to measure the thermal diffusivity. With this value, the thermal conductivity could be calculated where it was found the thermal conductivity consistently decreased as the GmB loading increased. This matches the hypothesis since glass acts as a thermal and conductive insulator. Finally, the composite materials were viewed under a high-power microscope to visualize the particle dispersion. At 400X the GmBs were able to be clearly seen and it was found they had an even dispersion at all loadings. Zooming to 2500X, CNTs were able to be seen where it was discovered they had decent dispersion but had many agglomerates which was determined to be caused by the mixing method.

Overall, it was determined that the CNT, GmB, and PDMS composite have good promise to be utilized as high temperature flexible sensors. The weight percentages of each additive could be tailored to match the specific use case. In the future it would be beneficial to use better mixing methods to vary the amount of CNTs in the composite and to increase the loading of GmB. Changing the amount of CNTs could possibly achieve better tensile and resistance properties allowing for better sensors to be made. Being able to increase the percent of GmBs has the ability to farther increase the thermal properties of the composite and even possibly increase resistive behaviors.

References

[1] V. Kostopoulos, A. Masouras, A. Baltopoulos, A. Vavouliotis, G. Sotiriadis, and L. Pambaguian, "A critical review of nanotechnologies for composite aerospace structures," *CEAS Space Journal,* vol. 9, pp. 35-57, 2017.

[2] J. Kupski and S. T. De Freitas, "Design of adhesively bonded lap joints with laminated CFRP adherends: Review, challenges and new opportunities for aerospace structures," *Composite Structures,* vol. 268, p. 113923, 2021.

[3] P. H. C. Camargo, K. G. Satyanarayana, and F. Wypych, "Nanocomposites: synthesis, structure, properties and new application opportunities," *Materials Research,* vol. 12, pp. 1-39, 2009.

[4] R. Yancey, "Challenges, opportunities, and perspectives on lightweight composite structures: aerospace versus automotive," *Lightweight composite structures in transport,* pp. 35-52, 2016.

[5] Y. Liu and S. Nayak, "Structural health monitoring: State of the art and perspectives," *Jom,* vol. 64, no. 7, pp. 789-792, 2012.

[6] V. Giurgiutiu, "Structural health monitoring of aerospace composites," 2015.

[7] G. F. Gomes, Y. A. D. Mendéz, P. d. S. L. Alexandrino, S. S. da Cunha Jr, and A. C. Ancelotti Jr, "The use of intelligent computational tools for damage detection and identification with an emphasis on composites–A review," *Composite Structures,* vol. 196, pp. 44-54, 2018.

[8] Y. Liu, M. Y. Fard, A. Chattopadhyay, and D. Doyle, "Damage assessment of CFRP composites using a time–frequency approach," *Journal of Intelligent Material Systems and Structures,* vol. 23, no. 4, pp. 397-413, 2012.

[9] Y. Liu, A. Rajadas, and A. Chattopadhyay, "A biomimetic structural health monitoring approach using carbon nanotubes," *Jom,* vol. 64, pp. 802-807, 2012.

[10] H. Zhou *et al.*, "Structural composite energy storage devices—a review," *Materials Today Energy,* vol. 24, p. 100924, 2022.

[11] M. Kessler, N. R. Sottos, and S. White, "Self-healing structural composite materials," *Composites Part A: applied science and manufacturing,* vol. 34, no. 8, pp. 743-753, 2003.

[12] J. S. M. Zanjani, B. S. Okan, P.-N. Pappas, C. Galiotis, Y. Z. Menceloglu, and M. Yildiz, "Tailoring viscoelastic response, self-heating and deicing properties of carbon-fiber reinforced epoxy composites by graphene modification," *Composites Part A: Applied Science and Manufacturing,* vol. 106, pp. 1-10, 2018.

[13] Z. K. Awad, T. Aravinthan, Y. Zhuge, and F. Gonzalez, "A review of optimization techniques used in the design of fibre composite structures for civil engineering applications," *Materials & Design,* vol. 33, pp. 534-544, 2012.

[14] M. Motavalli and C. Czaderski, "FRP composites for retrofitting of existing civil structures in Europe: State-of-the-art review," in *International Conference of Composites*

& Polycon, 2007: American Composites Manufacturers Association Tampa, FL, USA, pp. 17-19.
[15] S.-B. Park, E. Lih, K.-S. Park, Y. K. Joung, and D. K. Han, "Biopolymer-based functional composites for medical applications," *Progress in Polymer Science*, vol. 68, pp. 77-105, 2017.
[16] F. J. C. Braga, S. O. Rogero, A. A. Couto, R. F. C. Marques, A. A. Ribeiro, and J. S. d. C. Campos, "Characterization of PVDF/HAP composites for medical applications," *Materials Research*, vol. 10, pp. 247-251, 2007.
[17] S. A. Pineda-Castillo, J. Luo, H. Lee, B. N. Bohnstedt, Y. Liu, and C.-H. Lee, "Effects of Carbon Nanotube Infiltration on a Shape Memory Polymer-Based Device for Brain Aneurysm Therapeutics: Design and Characterization of a Joule-Heating Triggering Mechanism," *Advanced Engineering Materials*, vol. 23, no. 6, p. 2100322, 2021.
[18] J. Wang *et al.*, "Development of shape memory polymer nanocomposite foam for treatment of intracranial aneurysms," *Materials Letters*, vol. 250, pp. 38-41, 2019.
[19] C. Billings, P. Kim, T. Shadid, J. D. Ballard, C. Cai, and Y. Liu, "Implementation of Antibacterial Nanoparticles in Additive Manufacturing to Increase Part Strength and Stiffness," *Journal of Composites Science*, vol. 6, no. 9, p. 248, 2022.
[20] C. Billings, C. Cai, and Y. Liu, "Utilization of antibacterial nanoparticles in photocurable additive manufacturing of advanced composites for improved public health," *Polymers*, vol. 13, no. 16, p. 2616, 2021.
[21] M. A. Dheyab, A. A. Aziz, M. S. Jameel, O. A. Noqta, and B. Mehrdel, "Synthesis and coating methods of biocompatible iron oxide/gold nanoparticle and nanocomposite for biomedical applications," *Chinese Journal of Physics*, vol. 64, pp. 305-325, 2020.
[22] F. Fauzi, M. M. Musawwa, H. Hidayat, A. Kusumaatmaja, and W. S. B. Dwandaru, "Nanocomposites based on biocompatible polymers and graphene oxide for antibacterial coatings," *Polymers and Polymer Composites*, vol. 29, no. 9_suppl, pp. S1609-S1620, 2021.
[23] S. Sen, S. Patil, and D. S. Argyropoulos, "Thermal properties of lignin in copolymers, blends, and composites: a review," *Green Chemistry*, vol. 17, no. 11, pp. 4862-4887, 2015.
[24] J. Wang, P. Marashizadeh, B. Weng, P. Larson, M. C. Altan, and Y. Liu, "Synthesis, Characterization, and Modeling of Aligned ZnO Nanowire-Enhanced Carbon-Fiber-Reinforced Composites," *Materials*, vol. 15, no. 7, p. 2618, 2022.
[25] B. Herren, V. Webster, E. Davidson, M. C. Saha, M. C. Altan, and Y. Liu, "PDMS sponges with embedded carbon nanotubes as piezoresistive sensors for human motion detection," *Nanomaterials*, vol. 11, no. 7, p. 1740, 2021.
[26] B. Herren, M. C. Saha, and Y. Liu, "Carbon nanotube-based piezoresistive sensors fabricated by microwave irradiation," *Advanced Engineering Materials*, vol. 22, no. 2, p. 1901068, 2020.
[27] V. Mittal, *Synthesis techniques for polymer nanocomposites*. John Wiley & Sons, 2015.

[28] B. Herren, M. C. Saha, M. C. Altan, and Y. Liu, "Funnel-Shaped Floating Vessel Oil Skimmer with Joule Heating Sorption Functionality," *Polymers,* vol. 14, no. 11, p. 2269, 2022.
[29] P. Marashizadeh, M. Abshirini, M. Saha, L. Huang, and Y. Liu, "Atomistic Simulations on Structural Characteristics of ZnO Nanowire-Enhanced Graphene/Epoxy Polymer Composites: Implications for Lightweight Structures," *ACS Applied Nano Materials,* vol. 4, no. 11, pp. 11770-11778, 2021.
[30] M. Abshirini, M. Charara, P. Marashizadeh, M. C. Saha, M. C. Altan, and Y. Liu, "Functional nanocomposites for 3D printing of stretchable and wearable sensors," *Applied Nanoscience,* vol. 9, pp. 2071-2083, 2019.
[31] R. O. Rodrigues, R. Lima, H. T. Gomes, and A. M. Silva, "Polymer microfluidic devices: an overview of fabrication methods," *U. Porto Journal of Engineering,* vol. 1, no. 1, pp. 67-79, 2015.
[32] W. Luo, M. Charara, M. C. Saha, and Y. Liu, "Fabrication and characterization of porous CNF/PDMS nanocomposites for sensing applications," *Applied Nanoscience,* vol. 9, pp. 1309-1317, 2019.
[33] M. Charara, W. Luo, M. C. Saha, and Y. Liu, "Investigation of lightweight and flexible carbon nanofiber/poly dimethylsiloxane nanocomposite sponge for piezoresistive sensor application," *Advanced Engineering Materials,* vol. 21, no. 5, p. 1801068, 2019.
[34] M.-F. Yu, O. Lourie, M. J. Dyer, K. Moloni, T. F. Kelly, and R. S. Ruoff, "Strength and breaking mechanism of multiwalled carbon nanotubes under tensile load," *Science,* vol. 287, no. 5453, pp. 637-640, 2000.
[35] M. V. Kharlamova and C. Kramberger, "Applications of Filled Single-Walled Carbon Nanotubes: Progress, Challenges, and Perspectives," *Nanomaterials,* vol. 11, no. 11, p. 2863, 2021.
[36] R. Huang and P. Li, "Elastic behaviour and failure mechanism in epoxy syntactic foams: The effect of glass microballoon volume fractions," *Composites Part B: Engineering,* vol. 78, pp. 401-408, 2015.
[37] Y. Ozawa, M. Watanabe, T. Kikuchi, and H. Ishiwatari, "Mechanical and thermal properties of composite material system reinforced with micro glass balloons," in *IOP Conference Series: Materials Science and Engineering*, 2010, vol. 10, no. 1: IOP Publishing, p. 012094.
[38] Z. Li, S. Nambiar, W. Zheng, and J. Yeow, "PDMS/single-walled carbon nanotube composite for proton radiation shielding in space applications," *Materials Letters,* vol. 108, pp. 79-83, 2013.
[39] K. Efimenko, W. E. Wallace, and J. Genzer, "Surface modification of Sylgard-184 poly (dimethyl siloxane) networks by ultraviolet and ultraviolet/ozone treatment," *Journal of colloid and interface science,* vol. 254, no. 2, pp. 306-315, 2002.
[40] L. Vast *et al.*, "Multiwalled carbon nanotubes functionalized with 7-octenyltrichlorosilane and n-octyltrichlorosilane: dispersion in Sylgard® 184 silicone and Young's modulus," *Journal of materials science,* vol. 44, pp. 3476-3482, 2009.

[41] T. Srivastava, N. K. Katari, S. Krishna Mohan, C. Rama Krishna, and B. R. Ravuri, "Studies on Hollow Glass Microsphere Reinforced Silicone Matrix Composite for Use in Fast Curing Low Density Thermal Insulation Coating Applications," *Fibers and Polymers*, pp. 1-9, 2022.